Control Engineering Practice 78 (2018) 89–96

Contents lists available at ScienceDirect

Control Engineering Practice

journal homepage: www.elsevier.com/locate/conengprac

四旋翼

Contact force tracking of quadrotors based on robust attitude control

Carlos Izaguirre-Espinosa [a], Aldo-Jonathan Muñoz-Vázquez [b,*], Anand Sanchez-Orta [c], Vicente Parra-Vega [c], Pedro Castillo [d]

[a] Monterrey Institute of Technology and Higher Education (ITESM), Campus Sonora Norte, Hermosillo, Mexico
[b] Polytechnic University of Victoria (UPV), Ciudad Victoria, Mexico
[c] Robotics and Advanced Manufacturing Division, Research Center for Advanced Studies (CINVESTAV), Saltillo, Mexico
[d] Sorbonne Universités, Université de Technologie de Compiègne, CNRS UMR 7253 Heudiasyc Lab., CS 60319, 60203 Compiègne, France

ARTICLE INFO

Keywords:
Quadrotor UAV
Force control
Fractional-order control
Sliding mode control

ABSTRACT

Quadrotors are autonomous aerial vehicles widely developed in the last decade due to their small size, low weight and vertical take off and landing capabilities. Nowadays, some demanding applications involve the quadrotor interacting with rigid objects, requiring stable contact and force tracking. In this paper, an attitude control is proposed to handle force tracking by exploiting the high couplings among force, position and attitude dynamics. The proposed controller enforces a fractional sliding motion in finite-time to guarantee robust force tracking stabilisation in spite of disturbances and dynamical uncertainties. Experiments show additional theoretical and technological features to incorporate this flight mode in applications.

1. Introduction

Unmanned Aerial Vehicles (UAVs), such as quadrotors, have been employed in a wide range of applications thanks to their aerodynamic flight capabilities, (Sanchez-Orta, Parra-Vega, Izaguirre-Espinosa, & Garcia, 2015). However, the attitude stabilisation of quadrotors is by itself a non-trivial control problem, (Munoz-Vázquez, Parra-Vega, Sánchez-Orta, Garcia, & Izaguirre-Espinoza, 2014), which is exacerbated when the objective is position tracking because very fast attitude convergence is required to resolve under-actuation. Furthermore, it is clear that the force control problem is complicated because of the non-linear dependences and couplings among force, position and orientation coordinates, (Parra-Vega, Sanchez, Izaguirre, Garcia, & Ruiz-Sanchez, 2013). The quadrotor's force interaction problem has been addressed using a robotic end-effector to establish a contact point in Keemink, Fumagalli, Stramigioli, and Carloni (2012), though such solution is versatile, the coupled dynamics are neglected. Another approach, which also uses end-effectors, neglects the relation among attitude, thrust and exerted force, and assuming hovering and no aerodynamic effects, (Jimenez-Cano, Martin, Heredia, Ollero, & Cano, 2013). These studies show that a deep investigation on force quadrotor's dynamics is yet needed without introducing restrictive assumptions. In contrast, in this paper, and motivated by Izaguirre-Espinosa, Muñoz-Vázquez, Sánchez-Orta, Parra-Vega, and Castillo (2016) and Izaguirre-Espinosa, Muñoz-Vázquez, Sánchez-Orta, Parra-Vega, and Sanahuja (2016), a fractional sliding mode based controller is proposed to enforce robust force tracking, assuring $\mathcal{L}^2$ finite-gain input–output stability with respect to external disturbances and dynamical uncertainties. In addition, a quasi-hovering regime is not assumed, rather induced via the attitude controller.

The classical sliding mode control is robust to matched uncertainties, (Utkin, 1993), nevertheless, it suffers from chattering that may be unacceptable for some applications, such as rigid mechanical contact. To circumvent chattering, high-order sliding modes have been proposed based on the integral of a discontinuous function, (Damiano, Gatto, Marongiu, & Pisano, 2004; Pisano, Davila, Fridman, & Usai, 2008), however, at the expense of requiring differentiability of external disturbances, which is not always true in the general case of aerodynamic disturbances since they may render a non-smooth behaviour, (Humphrey, Schuler, & Rubinsky, 1992; Kolev, 2011; Kopasakis, 2012). To study robustness against this type of disturbances, (Muñoz-Vázquez, Parra-Vega, & Sánchez-Orta, 2015, 2016) propose a fractional sliding mode controller to provide a continuous control signal whose regularity is commensurable to the fractional order. From these studies, it is clear that fractional differintegral operators, (Podlubny, 1998), induce properties that are of interest for controlling some classes of complex dynamical systems, (Li & Hori, 2007; Tavazoei, Haeri, Jafari, Bolouki, & Siami, 2008), including mechanical plants, (Dumlu & Erenturk, 2014; Erenturk, 2013), and

* Corresponding author.
E-mail addresses: carlos.iza.es@itesm.mx (C. Izaguirre-Espinosa), amunozv@upv.edu.mx (A. Muñoz-Vázquez), anand.sanchez@cinvestav.mx (A. Sanchez-Orta), vparra@cinvestav.mx (V. Parra-Vega), castillo@hds.utc.fr (P. Castillo).

https://doi.org/10.1016/j.conengprac.2018.06.013
Received 5 March 2018; Received in revised form 5 May 2018; Accepted 23 June 2018

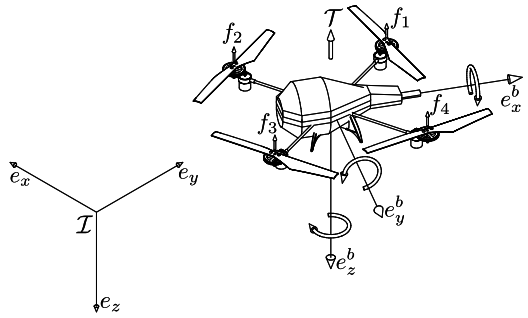

Fig. 1. The unconstrained quadrotor system and frames.

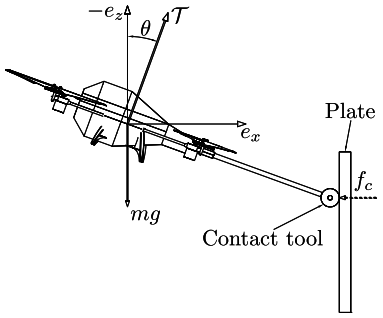

Fig. 2. The quadrotor system in constrained pose.

even quadrotors, (Munoz-Vázquez et al., 2014), and these properties provide more accurate tuning procedures, based on system and task specifications, (Badri & Tavazoei, 2015), while keeping in mind the regularity of the control signal, (Izaguirre-Espinosa, Muñoz-Vázquez, Sánchez-Orta, Parra-Vega, & Castillo, 2016; Izaguirre-Espinosa, Muñoz-Vázquez, Sánchez-Orta, Parra-Vega, & Sanahuja, 2016).

The fractional-order force–position controller proposed in this paper exhibits the following characteristics:

- Precise force tracking via robust attitude control
- A continuous controller that is robust to not necessarily differentiable aerodynamic disturbances
- Finite-gain input–output stability
- Real-time experiments

The rest of the paper is organised as follows: Section 2 addresses the dynamical model of a quadrotor in contact with a rigid object. Section 3 presents the attitude control design; then Section 4 introduces the force controller. An experimental study is discussed in Section 5, and main conclusions are given in Section 6.

2. Quadrotor dynamic model in contact

Consider a quadrotor in contact to a fixed object, and let $\mathcal{I} = \{e_x, e_y, e_z\}$ and $\mathcal{A} = \{e_x^b, e_y^b, e_z^b\}$ denote the inertial (Earth) and body fixed frames, respectively, as shown in Fig. 1. To obtain the dynamic equations that model the position and orientation coordinates, let the aircraft be represented as an airborne rigid body subject to one lift force and 3 moments, (Etkin & Reid, 1959). Consider also that the centre of mass (CoM) is located at the origin of $\mathcal{A}$ and fixed to the quadrotor, coinciding with its geometric centre.

The orientation of the rigid body is established by the rotation $\mathcal{R} : \mathcal{A} \longrightarrow \mathcal{I}$, where $\mathcal{R}(\eta) \in SO(3)$ is parametrised by Euler angles $\eta = (\phi, \theta, \psi)^T$, roll, pitch and yaw. The following Newton–Euler equations of motion model the dynamics of the quadrotor in contact to a fixed rigid body, see Fig. 2.

$$m\ddot{\xi} = -\mathcal{T}\mathcal{R}e_z + f_c + mge_z + d_\xi \tag{1}$$

$$\dot{\mathcal{R}} = \mathcal{R}[\Omega\times] \tag{2}$$

$$J\dot{\Omega} = -\Omega \times J\Omega + \tau + \vec{r}\times\mathcal{R}^T f_c + d_\eta \tag{3}$$

where $\xi = (x, y, z)^T \in \mathcal{I}$ denotes the position in $\mathcal{A}$, f_c stands for the contact force, $\Omega = (\Omega_1, \Omega_2, \Omega_3)^T \in \mathcal{A}$ represents the angular velocity expressed in the body fixed frame, $e_z = (0, 0, 1)^T$, $\mathcal{T} = f_1 + f_2 + f_3 + f_4 \in \mathbb{R}_+$ stands for the net thrust generated by each thruster as $f_i = \kappa_p\omega_i^2$, for $\kappa_p > 0$ a constant, and ω_i the angular velocity of each rotor; g represents the gravitational acceleration, $\vec{r}$ defines the vector from the centre of mass to the contact point, where f_c is exerted, m is the mass of the quadrotor, and $J \in \mathbb{R}^{3\times3}$ denotes the constant inertia matrix with respect to the CoM, expressed in $\mathcal{A}$. The term $[\Omega\times]$ denotes the skew-symmetric matrix of Ω, while d_ξ and d_η are external disturbances applied to the aerial vehicle, with $\tau \in \mathcal{A}$ the attitude control.

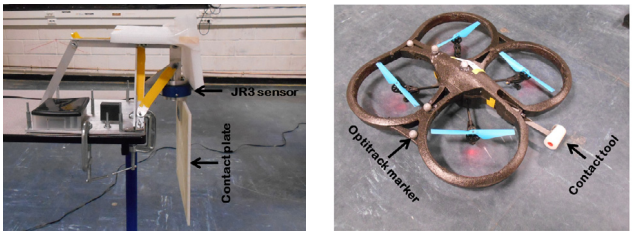

(a) The contact plate mounted on the force sensor.

(b) Parrot quadrotor with visual marks and contact tool.

Fig. 3. Experimental testbed.

The relationship between Ω and $\dot{\eta}$ is given by the linear map $W(\eta)$, in $\Omega = W(\eta)\dot{\eta}$, (Izaguirre-Espinosa, Muñoz-Vázquez, Sánchez-Orta, Parra-Vega, & Sanahuja, 2016). In addition, during contact, the quadrotor does not carry out any aggressive maneuver, however, it is preferred a singularity-free representation for attitude kinematics, thereby, consider Euler parameters represented by the unit-quaternion $\mathbf{q} = (q_0, q^T)^T \in \mathcal{S}^3$ such that $\mathbf{q}\otimes v\otimes\mathbf{q}^* = \mathcal{R}v \in \mathcal{I}$, $\forall v \in \mathcal{A}$, where $\mathbf{p}\otimes\mathbf{q} = (p_0q_0 - p^Tq, [p_0q + q_0p + p\times q]^T)^T$ is the quaternion product, and $\mathbf{q}^* = (q_0, -q^T)^T$ stands for the conjugated of $\mathbf{q} = (q_0, q^T)^T$. In addition, the time derivative of the unit-quaternion is (Sanchez-Orta et al., 2015),

$$\dot{\mathbf{q}} = \frac{1}{2}\begin{pmatrix} -q^T \\ q_0 I + [q\times] \end{pmatrix}\Omega. \tag{4}$$

3. Fractional sliding mode attitude control

The earth frame is chosen such that the exerted force is orthogonal to the z-axis in direction to the x-axis. Thus, in this design conditions the contact force can be controlled via the pitching angle θ and the thrust $\mathcal{T}$. According to this, the reference for the Euler angles is $\eta_d(t) = (0,\ \theta_d(t),\ 0)^T$, with $\theta_d(t)$ a function of the desired force. To design the attitude controller, let $\Omega_d = W(\eta_d)\dot{\eta}_d$ be the desired angular velocity, then (4) suggests to obtain the desired quaternion rate as

$$\dot{\mathbf{q}}_d = \frac{1}{2}\begin{pmatrix} -q_d^T \\ q_{0d} I + [q_d\times] \end{pmatrix}\Omega_d. \tag{5}$$

Consequently, it results

$$\dot{\mathbf{q}}_e = \frac{1}{2}\begin{pmatrix} -q_e^T \\ q_{0e} I + [q_e\times] \end{pmatrix}\mathcal{R}_d\Omega_e, \tag{6}$$

for $\mathbf{q}_e = \mathbf{q}\otimes\mathbf{q}_d^*$ the quaternion error, $\mathcal{R}_d$ the desired rotation and $\Omega_e = \Omega - \Omega_d$. Now, similarly to Izaguirre-Espinosa, Muñoz-Vázquez, Sánchez-Orta, Parra-Vega, and Castillo (2016), consider the extended error manifold

$$S_\Omega = \Omega_e + \alpha\mathcal{R}_d^T q_e, \tag{7}$$

for constant $\alpha > 0$. Clearly, notice that if $S_\Omega = 0$ then $\mathbf{q}_e \to (1,0)^T$ exponentially, (Sanchez-Orta et al., 2015), and therefore, $\eta \to \eta_d$. Thus, consider the ith entry of the following open-loop attitude error equation, using (3),

$$J_{ii}\dot{S}_{\Omega i} = \tau_i + d_{\Omega i} \tag{8}$$

where $d_{\Omega i} = d'_{\Omega i} + \sum_{j\neq i} J_{ij}\dot{S}_{\Omega j}$, for $d'_\Omega = -J\dot{\Omega}_r - \Omega \times J\Omega + \vec{r}\times\mathcal{R}^T f_c + d_\eta$ and $\Omega_r = \Omega_d - \alpha\mathcal{R}_d^T q_e$, including for endogenous and exogenous disturbances.

The control objective is the designing of a continuous τ_i in (8) to enforce the invariant $S_{\Omega i} = 0$ in finite-time. Thus, as in Izaguirre-Espinosa, Muñoz-Vázquez, Sánchez-Orta, Parra-Vega, and Castillo (2016), consider the ith entry of the attitude controller,

$$\tau_i = -k\ {}_{t_{ni}}I_t^\nu \mathrm{sign}(S_{\Omega i}), \tag{9}$$

with $k > 0$ a feedback gain, and t_{ni} every instant at $S_{\Omega i}(t_{ni}) = 0$, and the Riemann–Liouville operator (Podlubny, 1998),

$${}_aI_t^\nu f(t) = \frac{1}{\Gamma(\nu)}\int_a^t (t-\varsigma)^{\nu-1} f(\varsigma)d\varsigma$$

that stands for a fractional integral of order $\nu \in [0,1)$ of the locally integrable function $f(t)$, with $\Gamma(\nu)$ the Gamma function, that is $\Gamma(\nu+1) = \nu!$ for $\nu \in \mathbb{N}_0$. The stability of (8) in closed loop with (9) is analysed in the following theorem, whose proof have been presented in Izaguirre-Espinosa, Muñoz-Vázquez, Sánchez-Orta, Parra-Vega, and Castillo (2016).

Theorem 1. *Consider (8) closed by (9). For feedback gain* $k > \frac{3+\nu}{1-\nu}\sup_{(a,b),i}\frac{|d_{\Omega i}(b)-d_{\Omega i}(a)|}{(b-a)^\nu}$, $\exists t_f < \infty$ *such that* $S_\Omega(t) = 0$, $\forall t \geq t_f$.

Theorem 1 implies that after t_f, $\phi = \psi = 0$ and $\theta = \theta_d$ is guaranteed asymptotically, invariantly to the effect of non-differentiable disturbances, (Izaguirre-Espinosa, Muñoz-Vázquez, Sánchez-Orta, Parra-Vega, & Castillo, 2016; Muñoz-Vázquez et al., 2015). Note that the fractional integral acts as a low-pass filter, whose gain and phase can be modulated via $\nu \in [0,1)$.

4. Force control design

The challenge is the tracking of contact force f_c orthogonal to the z-axis, and along x. Assuming stable contact initial condition, the attitude control τ induces a quasi-hovering state. The impact transition control consists in a fast dissipation of the impact energy, which is obtained by adding a high damping action during the phase transition, however, the transition analysis is beyond the scope of this paper, and has been treated in Khatib and Burdick (1986) and Marth, Tarn, and Bejczy (1993). Thus, the force–position dynamics is given by

$$m\ddot{x} = -\mathcal{T}\sin(\theta) + f_x + d_x \tag{10}$$

$$m\ddot{z} = -\mathcal{T}\cos(\theta) + mg + d_z \tag{11}$$

where f_x represents the magnitude and direction of the contact force, and d_x and d_z are unknown disturbances. The dynamics of y is stabilised via ψ, then, by combining Eqs. (10) and (11), one obtains

$$\tan(\theta) = \frac{f_x - m\ddot{x} + d_x}{m(g-\ddot{z}) + d_z}. \tag{12}$$

In addition, one can write

$$\theta = \frac{f_x}{mg} + d_\theta, \tag{13}$$

for $d_\theta = \frac{mg(d_x - m\ddot{x}) + (m\ddot{z} - d_z)f_x}{mg[m(g-\ddot{z})+d_z]} + [\theta - \tan(\theta)]$. Noticing that θ depends on f_x, establishing that θ_d can be proposed as a function of the desired contact force f_{xd}. Now, assume that $\ddot{x} \approx \ddot{z} \approx 0$ and $\tan(\theta) \approx \theta$, to attenuate the effect of d_θ. This is physically reasonable because otherwise the quadrotor cannot compensate its own weight, let alone to apply a desired force. Henceforth, the desired pitching angle becomes

$$\theta_d = \frac{f_{xd}}{mg}. \tag{14}$$

Thus,

$$\Delta\theta = \frac{\Delta f_x}{mg} + d_\theta \tag{15}$$

where $\Delta\theta = \theta - \theta_d$ and $\Delta f_x = f_x - f_{xd}$.

The classical scheme of stiffness establishes that $\Delta f_x = -k_f \Delta x_p$, for constant k_f, with x_p and x_{pd} the penetration and the reference inside the object, and $\Delta x_p = x_p - x_{pd}$. Note that during the quadrotor being in contact, one has

$$\begin{aligned} x &= x_c + x_p - r\cos(\theta) \\ z &= z_c + r\sin(\theta) \end{aligned} \tag{16}$$

where x_c and z_c stand for the contact point in the x and z axis, respectively, and r is the distance from the contact point to the centre of mass of the quadrotor. Then, it is evident that the position and force dynamics are stabilised directly by controlling θ.

Since the attitude controller enforces the fast convergence of $\eta \approx 0$, it follows that $q \approx \frac{1}{2}\eta$, and $R \approx W \approx I$; then, (7) can be approximated by

$$S_\Omega = \Delta\dot{\eta} + \frac{1}{2}\alpha\Delta\eta, \tag{17}$$

with $\Delta\eta = \eta - \eta_d$. Replacing the second term of (17) by

$$S_f = \Delta\dot{\theta} + \frac{\alpha}{2mg}\Delta f_x, \tag{18}$$

the controller

$$\tau_\theta = -k\ {}_{t_{nf}}I_t^\nu \mathrm{sign}(S_f), \tag{19}$$

for t_{nf} the time instant at $S_f(t_{nf}) = 0$, induces the sliding motion $S_f = 0$ in finite-time. Then, one obtains, as a direct consequence of Theorem 1, the following main result.

Theorem 2. *Consider the second-entry of vector-control τ is given by (19), with S_f in (18). Then, for a sufficiently small initial condition $\eta(t_0)$, one obtains that*

$$\|\Delta f_x\|_{\mathcal{L}^2} \leq (2mg/\alpha)\|\dot{d}_\theta\|_{\mathcal{L}^2} \tag{20}$$

for the zero-state response of Δf_x.

Proof. In virtue of Theorem 1, $S_f = 0$ in finite-time, then,

$$\Delta\dot{f}_x + (\alpha/2)\Delta f_x + mg\dot{d}_\theta = 0.$$

Thus, taking the Fourier transform of the zero-state response produces

$$\mathcal{F}\{\Delta f_x\} = -G(j\omega)\mathcal{F}\{\dot{d}_\theta\}$$

where $G(j\omega) = \frac{mg}{j\omega + \alpha/2}$. Then,

$$\|\Delta f_x\|_{\mathcal{L}^2} \leq \|G(j\omega)\|_{\mathcal{H}^\infty}\|\dot{d}_\theta\|_{\mathcal{L}^2} = (2mg/\alpha)\|\dot{d}_\theta\|_{\mathcal{L}^2},$$

consequently, the force tracking is finite-gain input–output stable, whose sensitivity against exogenous disturbances and uncertainties can be tuned via α. □

Theorem 2 states that the precision of the force tracking can be modulated via α. The use of $\dot{\theta}(t)$ instead of $\dot{f}_x(t)$ sacrifices the exponential convergence of $\Delta f_x(t)$ just obtaining finite-gain input–output stability, (Zames, 1966), but from a practical point of view, signal $\dot{\theta}(t)$ is more regular than signal $f_x(t)$. Then, the consequence of Theorem 2 is not imposed by simplicity rather an implicit consequence of the way that the force tracking problem is addressed since it is not physically possible making pirouette while exerting a desired force onto a rigid wall.

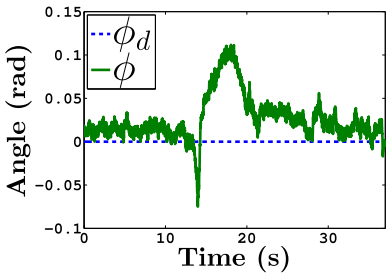

(a) Regulation at $\phi_d = 0$ suffers from force disturbances.

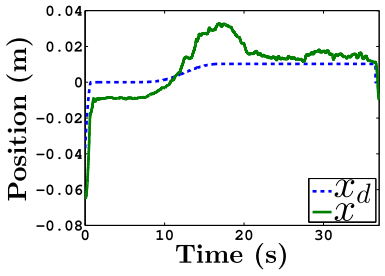

(b) Tracking of smooth reference in x axis.

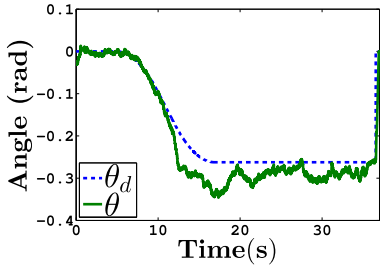

(c) Tracking of smooth θ_d leads to force regulation.

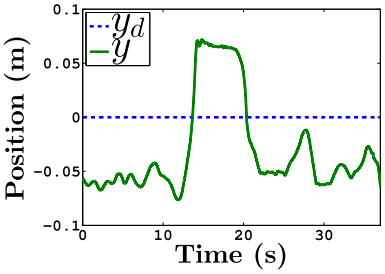

(d) Regulation in y axis heavily affected by force disturbance.

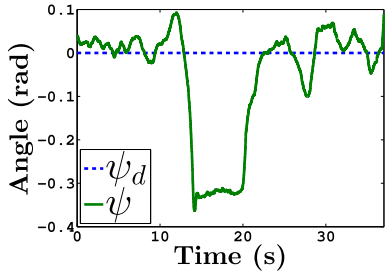

(e) Regulation in ψ suffers the most due to force and torques disturbances.

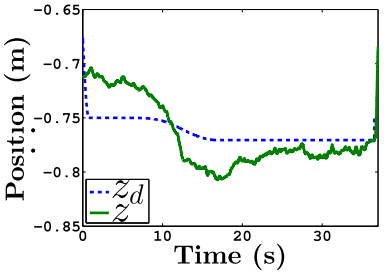

(f) Tracking in z axis.

Fig. 4. Quadrotor performance for Experiment A.

5. Experimental study

Experiments were conducted in the Heudiasyc Laboratory at the *Université de Technologie de Compiègne*. https://www.youtube.com/watch?v=o9g3jacwZSU. Initially, the quadrotor flights in free motion towards a contact plate to establish stable contact using the tracking controller (Izaguirre-Espinosa, Muñoz-Vázquez, Sánchez-Orta, Parra-Vega, & Sanahuja, 2016), then the force experiment starts. Two experiments are considered:

- Experiment A: Force regulation
- Experiment B: Force tracking

5.1. Experimental setup

The experimental platform consists of a Parrot AR Drone 2.0 as the quadrotor UAV, an Optitrack motion capture system, which provides inertial Cartesian coordinates and Euler angles, and a JR3 multi-axis load cell force sensor. The Parrot is surrounded with a styrofoam, which protects the quadrotor efficiently against collisions that are abundant in force control flight tests. Two desktop ground PCs run three process, one PC provides Optitrack data at about 100 Hz and wireless communications to the Parrot AR throughout Gumstix processing ports, while another PC handles the 90M31 JR3 force and moment data throughout a dedicated PCI-based DSP board at 1KHz with a second order filter. The Parrot quadrotor weighs 0.458 kg, which limits the amount of force exerted on the environment, given that there exists a direct relation between weight and force variables.

The autonomy of the Parrot in force flight mode is affected dramatically by force disturbances, as well as battery charge, which when in nominal initial full charge renders appropriately for about 10 min before degrading its delivery of current demanded by the control algorithm. Control code is embedded on-board the quadrotor using a Gumstix architecture in C++ using Codeblocks in a Linux Mint environment, also, the on-board Gumstix handles control interrupts and communication as well. It is important to mention that we have developed a software framework that allows the control algorithms to be directly implemented using only the hardware of the Parrot. The Optitrack measures ψ directly while ϕ and θ are computed based on a data fusion with the inertial measurement unit (IMU) at 100 Hz, closing the control algorithm at 10 ms.

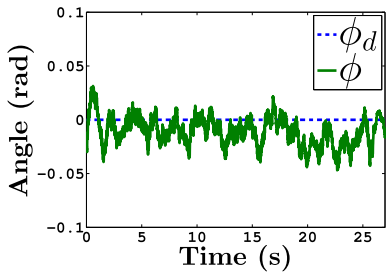

(a) Regulation $\phi_d = 0$, is less disturbed than Experiment A.

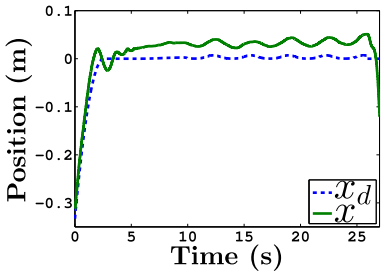

(b) Tracking of smooth reference in x axis allows force exertion.

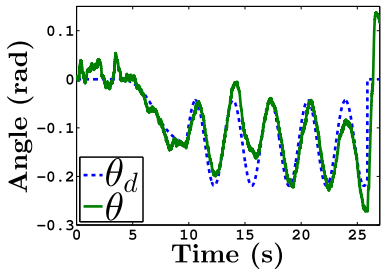

(c) Tracking of a sine function in θ allows force tracking.

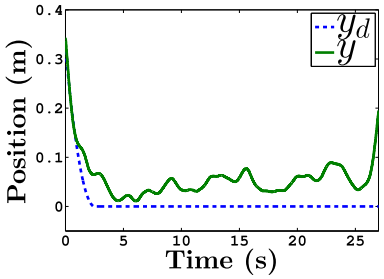

(d) Regulation in y axis heavily affected by force disturbance.

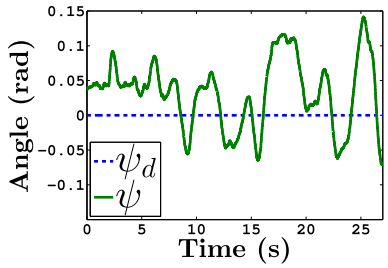

(e) Due to the force tracking, the regulation in ψ suffers more from disturbances.

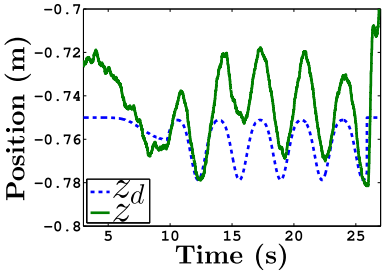

(f) Tracking in z axis.

Fig. 5. Quadrotor performance for Experiment B.

The Grünwald–Letnikov method is coded to compute numerical differintegrals with a maximum of 5000 memory elements at each iteration. As usual in practice, desired flight regime is watched so as to avoid control saturations, that if happens, it is set to the maximum and minimum bits allowed by the rotors speed before saturating the mapping to the rotor's drivers, *i.e.* the sum of all attitude control inputs is constrained to $\tau_\phi + \tau_\theta + \tau_\psi \leq 1$.

Fig. 3(a) shows the contact plate made of Nylamid, and mounted rigidly on a JR3 aluminium fixture. The plate is localised, such that, the applied force is measured along the positive direction of x. The carbon fibre contact tool in Fig. 3(b) is rigidly attached to the frame in a × configuration at 45° of axis, whose tip is a rigid rod surrounded with sponge to facilitate mechanical contact. In order to handle the rattle between the contact tool and the sensor plate, the approaching phase to the contact point happens smoothly and slowly thanks to the desired position reference, and once in position, an offset in θ of 2° is put into action to guarantee the contact.

5.2. Experimental conditions and feedback gain tuning

For Experiment A, the flight test corresponds to regulation of constant force in a rigid plate at contact point $[x_c, y_c, z_c] = [0, 0, -0.75]$ m. For regulation at $f_d = 1.33$ N, a smooth trajectory is in place from $f_d(t_0) = 0$ N. This corresponds to regulate at $\theta_d = -15°$, with $[x_d, y_d, z_d] = [0.01, 0, -0.77]$ m.

For Experiment B, the force tracking, once the quadrotor is in stable contact with the plate, firstly, it goes smoothly to $f_d = 0.6267$ N corresponding to $\theta_d = -7.5°$ at $[x, y, z] = [0.002, 0, -0.7603]$ m. From there, it tracks $f_{x_d}(t) = 0.6267 - 0.4178\sin(t - 9.768)$ N that corresponds to $\theta_d(t) = -0.1309 + 0.0873\sin(t - 9.768)$rad. In summary, the quadrotor slowly tilts in θ until it reaches $-7.5°$, then, it tracks a sine with an amplitude of 5°.

Feedback gains are $\nu = 0.6$, $\alpha = 9$ and $k = 0.6$ for both experiments. It is important to notice that the differintegration order ν plays a critical part not only in the disturbance rejection problem but also in how regular the control signal is. For instance, for $\nu = 0.5$, the control signal is barely continuous in practice, but for $\nu < 0.5$, the regularity of the

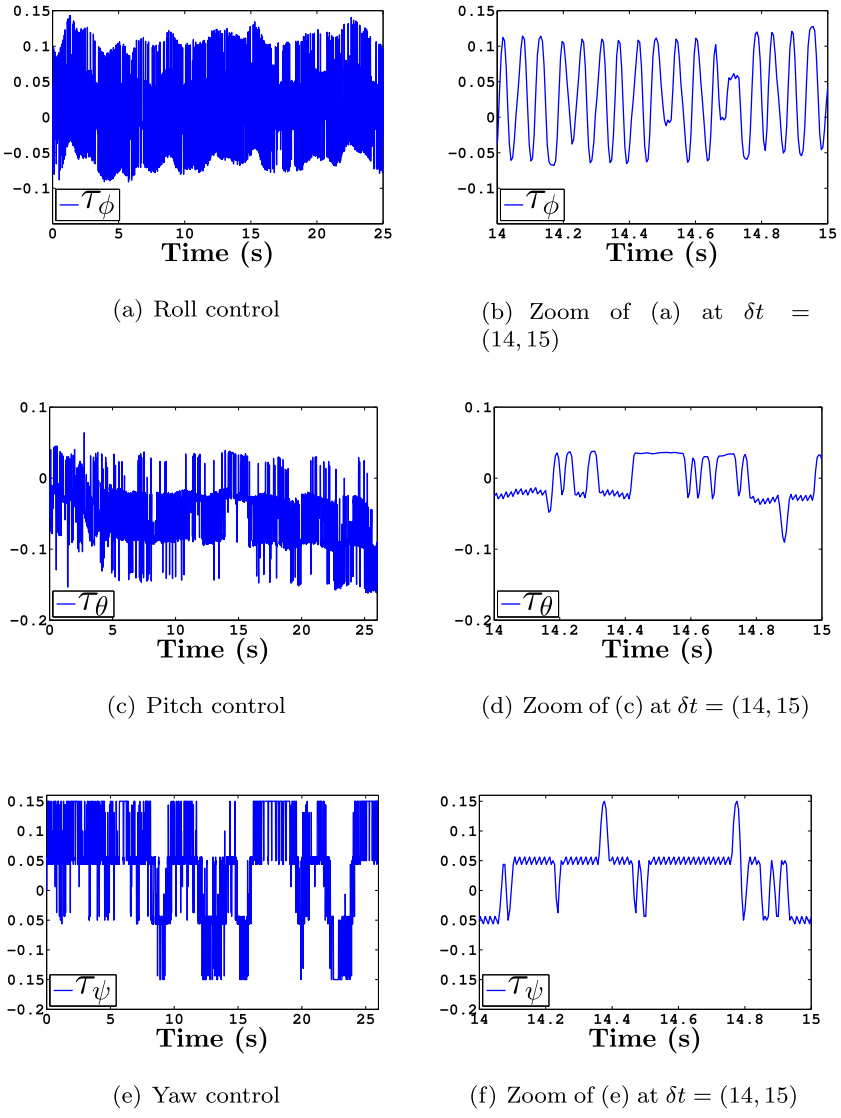

(a) Roll control

(b) Zoom of (a) at $\delta t = (14, 15)$

(c) Pitch control

(d) Zoom of (c) at $\delta t = (14, 15)$

(e) Yaw control

(f) Zoom of (e) at $\delta t = (14, 15)$

Fig. 6. Experiment B: Control signals (in Nm), and a zoom in right column figures.

control signal degenerates into a very aggressive high frequency signal, resembling to chattering of the classical sliding modes that endangers the integrity of rotors. Moreover, $\nu > 0.7$ creates a phase delay high enough that destabilises the quadrotor beyond recovery.

5.3. Experimental results

Experimental data show successful results of force control in rigid contact regime, previously unreported in literature. Figs. 4(e) and 5(e) show how difficult regulation of ψ is, due to the yawing moment resulting from the mechanical vibration of the quadrotor that also makes hard to regulate at $y_d = 0$, see Figs. 4(d) and 5(d). This difficulty arises from the geometry of the contact tool since it is a rod. In fact, there are some disturbances that affect the quadrotor in such a way that the contact tool tip starts to tilt to the right or left and the line of contact of the rod becomes a point in one of its edges. This disturbance is rejected by tilting the quadrotor in the opposite direction, trying to recover the line of contact. It can be seen in experiments how this phenomenon can quickly drain the quadrotor battery if the controller is not well tuned. Also, when f_{xd} is incremented, so does the yawing moment, which may destabilise the quadrotor due to the limited energy available during contact to deal with disturbances. The tracking of x_d and z_d is presented in Figs. 4(b), (f), 5(b) and (f), where the coupled compliant behaviour of position tracking can be appreciated.

From Fig. 7(a) and (b), despite showing successful force tracking, it can be seen that the high frequency mechanical vibrations of the quadrotor frame, corresponding to high rotational velocity of thrusters, affect directly the experiments.

In addition to the previous problems, it is important to note that the desired position and attitude references are calculated using the distance between the tool tip and the centre of mass of the quadrotor. However, in experiments, this distance was measured from the tool tip to the centre of the quadrotor, which originates a parametric uncertainty affecting the desired position and attitude references, according to (16). As a result, the corresponding attitude and position reference signals compliant with the desired force are slightly different from the ones calculated in practice. In spite of this problem, it can be seen from Fig. 7 that the force reference is being tracked with enough accuracy to make some quadrotor interaction tasks possible, which is the main goal of the proposed approach.

Fig. 6 shows the continuous control signals that are easily handled by the UAV rotors.

Finally, the attitude sliding surfaces remain around zero to witness the enforcement of the sliding mode, see Fig. 8(a) and (b), despite of unforeseen disturbances originated from the vibrating quadrotor

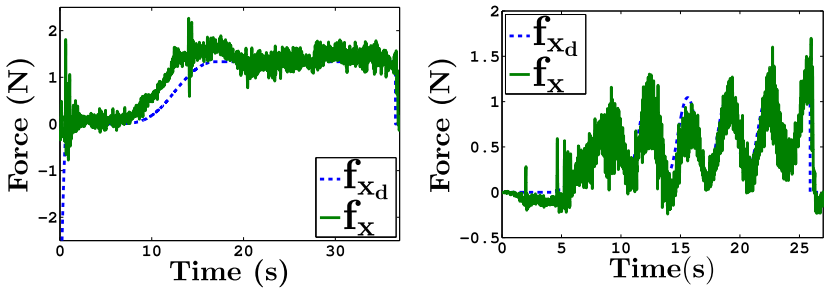

(a) Force regulation at 1.33 N (b) Force tracking of a sine

Fig. 7. Regulation and tracking of force, for each experiments.

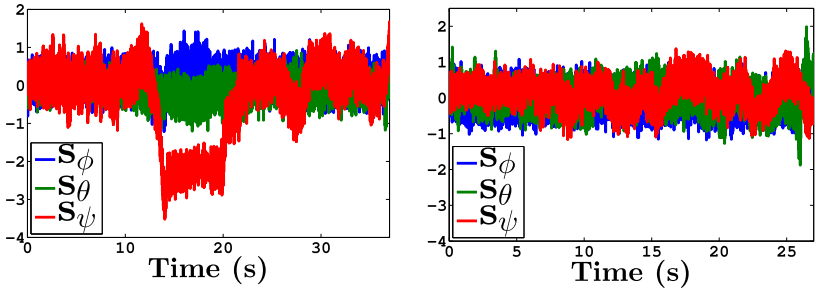

(a) Sliding surfaces for regulation (b) Sliding surfaces for tracking

Fig. 8. Sliding surfaces, for each experiment.

mechanically coupled to the rigid plate, induced disturbances of contact forces and moments, as well as noisy measurement.

Remark 1. The unavoidable non-zero tracking error is inherent to this type of applications, and is caused not only by limited sampling rate, multi-sampling, sensors resolution, noisy measurements, latencies, and quantisation, typical of this sort of experiments, but, most importantly, by the highly coupled aerodynamics of the quadrotor, and the battery discharge dynamics, which affects the behaviour of the forces generated by the rotors, as well as the high-frequency vibrations induced by the rotors' motion, which in turn introduce high-frequency noise to the force sensor. Some of these problems can be solved as technology advances, such as battery, hardware, firmware, and software, and some of them are relevant open problems, such as quantisation and delays on states and inputs, where important results have been reported in the literature (Mirkin & Gutman, 2010; Persis & Mazenc, 2010; Ye, 2011; Zhou & Yang, 2014), however, they are beyond the scope of this manuscript.

6. Conclusions

It was shown that force control along the under-actuated translational axes implies to resolve explicitly under-actuation, but not only that, in practice, it stands as a harder problem due to the mechanical vibrations involved. Our proposal enforces fractional sliding modes in finite-time, which facilitates to solve under-actuation and to analyse how endogenous and exogenous aerodynamic disturbances influence the system response. Interestingly, but somehow expected, there appears a relation of the applied force and attitude, suggesting that the force controller can be expressed in terms of the attitude reference signals. Experiments show that in constrained motion, not only a fast and robust attitude–force controller is required, but due to reaction torques and high frequency mechanical vibrations, a very high sampling rate is a requirement. This represents a control challenge, from theoretical and practical point of view. Moreover, there also exists an aerodynamic limitation on how much force can be exerted, not only from the capacity of thrusters but because tilt increases as the desired force does, then, it must be careful computed otherwise quadrotor may stall. Our complete algorithm was proved and experimentally tested to be of computationally low cost, showing a robust force regulation and tracking. In order to increase the force degrees of freedom, it is proposed as a future work to study the soft finger-tip model in force interaction, similar to Garcia-Rodriguez, Segovia-Palacios, and Villalva-Lucio (2016). Firstly, because it will greatly dampen the vibrations of the quadrotor in contact, and secondly, because using a soft finger-tip as the contact tool will increase the capabilities of the quadrotor to apply force in two dimensions, of course, several challenges will have to be overcome in the controller to manage at the same time the tangential and normal components of the force.

Acknowledgements

Authors acknowledge partial support from Conacyt-Mexico under Research Grants 264513, 133344 and 133546. This work has been sponsored by the French government research program "Investissements d'avenir" through the Robotex Equipment of Excellence (ANR-10-EQPX-44). This work was carried out in the framework of the Labex MS2T, which was funded by the French Government, through the program "Investments for the future" managed by the National Agency for Research (Reference ANR-11-IDEX-0004-02).

References

Badri, V., & Tavazoei, M. S. (2015). Achievable performance region for a fractional-order proportional and derivative motion controller. *IEEE Transactions on Industrial Electronics*, *62*(11), 7171–7180.

Damiano, A., Gatto, G. L., Marongiu, I., & Pisano, A. (2004). Second-order sliding-mode control of dc drives. *IEEE Transactions on Industrial Electronics*, *51*(2), 364–373.

Dumlu, A., & Erenturk, K. (2014). Trajectory tracking control for a 3-dof parallel manipulator using fractional-order $PI^{\lambda}D^{\mu}$ control. *IEEE Transactions on Industrial Electronics*, *61*(7), 3417–3426. http://dx.doi.org/10.1109/TIE.2013.2278964.

Erenturk, K. (2013). Fractional-order $PI^{\lambda}D^{\mu}$ and active disturbance rejection control of nonlinear two-mass drive system. *IEEE Transactions on Industrial Electronics*, *60*(9), 3806–3813.

Etkin, B., & Reid, L. D. (1959). *Dynamics of flight*. Wiley New York.

Garcia-Rodriguez, R., Segovia-Palacios, V., Parra-Vega, V., Villalva-Lucio, M. (2016). *Dynamic optimal grasping of a circular object with gravity using robotic soft-fingertips, Vol. 26* (pp. 309–323).

Humphrey, J., Schuler, C., & Rubinsky, B. (1992). On the use of the weierstrass-mandelbrot function to describe the fractal component of turbulent velocity. *Fluid Dynamics Research*, *9*(1–3), 81–95.

Izaguirre-Espinosa, C., Muñoz-Vázquez, A. J., Sánchez-Orta, A., Parra-Vega, V., & Castillo, P. (2016). Attitude control of quadrotors based on fractional sliding modes: theory and experiments. *IET Control Theory & Applications*, *10*(7), 825–832.

Izaguirre-Espinosa, C., Muñoz-Vázquez, A., Sánchez-Orta, A., Parra-Vega, V., & Sanahuja, G. (2016). Fractional attitude-reactive control for robust quadrotor position stabilization without resolving underactuation. *Control Engineering Practice*, *53*, 47–56.

Jimenez-Cano, A., Martin, J., Heredia, G., Ollero, A., & Cano, R. (2013). Control of an aerial robot with multi-link arm for assembly tasks. In *Robotics and automation, 2013 IEEE international conference on* (pp. 4916–4921). IEEE.

Keemink, A. Q., Fumagalli, M., Stramigioli, S., & Carloni, R. (2012). Mechanical design of a manipulation system for unmanned aerial vehicles. In *Robotics and automation, 2012 IEEE international conference on* (pp. 3147–3152). IEEE.

Khatib, O., Burdick, J. (1986). Motion and force control of robot manipulators. In *Robotics and Automation. Proceedings. 1986 IEEE International Conference on, Vol. 3*. IEEE (pp. 1381–1386).

Kolev, N. I. (2011). *Multiphase flow dynamics 3: Thermal interactions, Vol. 3*. Springer Science & Business Media.

Kopasakis, G. (2012). Modeling of atmospheric turbulence as disturbances for control design and evaluation of high speed propulsion systems. *Journal of Dynamic Systems, Measurement, and Control*, *134*(2), 021009.

Li, W., & Hori, Y. (2007). Vibration suppression using single neuron-based pi fuzzy controller and fractional-order disturbance observer. *IEEE Transactions on Industrial Electronics*, *54*(1), 117–126.

Marth, G., Tarn, T. J., & Bejczy, A. K. (1993). Stable phase transition control for robot arm motion. In *IEEE International Conference on Robotics and Automation* (pp. 355–362). IEEE.

Mirkin, B., & Gutman, P. (2010). Robust adaptive output-feedback tracking for a class of nonlinear time-delayed plants. *IEEE Transactions on Automatic Control*, *55*(10), 2418–2424.

Muñoz-Vázquez, A., Parra-Vega, V., & Sánchez-Orta, A. (2015). Continuous fractional sliding mode-like control for exact rejection of non-differentiable hölder disturbances. *IMA Journal of Mathematical Control and Information*, *34*(2), 597–610.

Muñoz-Vázquez, A.-J., Parra-Vega, V., & Sánchez-Orta, A. (2016). Uniformly continuous differintegral sliding mode control of nonlinear systems subject to hölder disturbances. *Automatica*, *66*, 179–184.

Munoz-Vázquez, A.-J., Parra-Vega, V., Sánchez-Orta, A., Garcia, O., & Izaguirre-Espinoza, C. (2014). Attitude tracking control of a quadrotor based on absolutely continuous fractional integral sliding modes. In *Control applications, 2014 IEEE conference on* (pp. 717–722). IEEE.

Parra-Vega, V., Sanchez, A., Izaguirre, C., Garcia, O., & Ruiz-Sanchez, F. (2013). Toward aerial grasping and manipulation with multiple uavs. *Journal of Intelligent and Robotic Systems*, *70*(1–4), 575–593.

Persis, C. D., & Mazenc, F. (2010). Stability of quantized time-delay nonlinear systems: a Lyapunov-Krasowskii-functional approach. *Mathematics of Control, Signals, and Systems*, *21*(4), 337–370.

Pisano, A., Davila, A., Fridman, L., & Usai, E. (2008). Cascade control of pm dc drives via second-order sliding-mode technique. *IEEE Transactions on Industrial Electronics*, *55*(11), 3846–3854.

Podlubny, I. (1998). *Fractional differential equations: An introduction to fractional derivatives, fractional differential equations, to methods of their solution and some of their applications, Vol. 198*. Elsevier.

Sanchez-Orta, A., Parra-Vega, V., Izaguirre-Espinosa, C., & Garcia, O. (2015). Position-yaw tracking of quadrotors. *Journal of Dynamic Systems, Measurement, and Control*, *137*(6), 061011.

Tavazoei, M. S., Haeri, M., Jafari, S., Bolouki, S., & Siami, M. (2008). Some applications of fractional calculus in suppression of chaotic oscillations. *IEEE Transactions on Industrial Electronics*, *55*(11), 4094–4101.

Utkin, V. I. (1993). Sliding mode control design principles and applications to electric drives. *IEEE Transactions on Industrial Electronics*, *40*(1), 23–36.

Ye, X. (2011). Decentralized adaptive stabilization of large-scale nonlinear time-delay systems with unknown high-frequency-gain signs. *IEEE Transactions on Automatic Control*, *56*(6), 1473–1478.

Zames, G. (1966). On the input–output stability of time-varying nonlinear feedback systems part one: Conditions derived using concepts of loop gain, conicity, and positivity. *IEEE Transactions on Automatic Control*, *11*(2), 228–238.

Zhou, C. W. J., & Yang, G. (2014). Adaptive backstepping stabilization of nonlinear uncertain systems with quantized input signal. *IEEE Transactions on Automatic Control*, *59*(2), 460–464.